DIGITAL ACCESS TO SCHOLARSHIP AT HARVARD
DASH.HARVARD.EDU

HARVARD LIBRARY
Office for Scholarly Communication

# Real-Time Nanoparticle–Cell Interactions in Physiological Media by Atomic Force Microscopy

**Citation**
Pyrgiotakis, Georgios, Christoph O. Blattmann, and Philip Demokritou. 2014. "Real-Time Nanoparticle–Cell Interactions in Physiological Media by Atomic Force Microscopy." ACS Sustainable Chemistry & Engineering 2 (7): 1681-1690. doi:10.1021/sc500152g. http://dx.doi.org/10.1021/sc500152g.

**Published Version**
doi:10.1021/sc500152g

**Permanent link**
http://nrs.harvard.edu/urn-3:HUL.InstRepos:17295579

**Terms of Use**
This article was downloaded from Harvard University's DASH repository, and is made available under the terms and conditions applicable to Other Posted Material, as set forth at http://nrs.harvard.edu/urn-3:HUL.InstRepos:dash.current.terms-of-use#LAA

## Share Your Story

The Harvard community has made this article openly available.
Please share how this access benefits you. Submit a story .

Accessibility

ACS Sustainable Chemistry & Engineering

Research Article

pubs.acs.org/journal/ascecg

Terms of Use

# Real-Time Nanoparticle–Cell Interactions in Physiological Media by Atomic Force Microscopy

Georgios Pyrgiotakis, Christoph O. Blattmann, and Philip Demokritou*

Center for Nanotechnology and Nanotoxicology at Harvard School of Public Health, Harvard University, 665 Huntington Avenue, 02115 Boston, Massachusetts United States

Supporting Information

**ABSTRACT:** Particle–cell interactions in physiological media are important in determining the fate and transport of nanoparticles and biological responses to them. In this work, these interactions are assessed in real time using a novel atomic force microscopy (AFM) based platform. Industry-relevant $CeO_2$ and $Fe_2O_3$ engineered nanoparticles (ENPs) of two primary particle sizes were synthesized by the flame spray pyrolysis (FSP) based Harvard Versatile Engineering Nanomaterials Generation System (Harvard VENGES) and used in this study. The ENPs were attached on AFM tips, and the atomic force between the tip and lung epithelia cells (A549), adhered on a substrate, was measured in biological media, with and without the presence of serum proteins. Two metrics were used to assess the nanoparticle cell: the detachment force required to separate the ENP from the cell and the number of bonds formed between the cell and the ENPs. The results indicate that these atomic level ENP–cell interaction forces strongly depend on the physiological media. The presence of serum proteins reduced both the detachment force and the number of bonds by approximately 50% indicating the important role of the protein corona on the particle cell interactions. Additionally, it was shown that particle to cell interactions were size and material dependent.

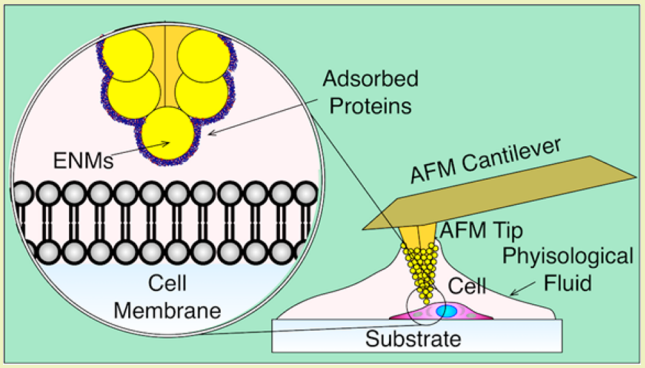


**KEYWORDS:** *Nanoparticles, Nanotoxicology, Protein corona, Atomic force microscopy, Cerium oxide, Iron oxide, Nano-EHS, Nano–bio interactions*

## INTRODUCTION

The use of engineered nanoparticles (ENPs) in many commercial products and their involvement in many industrial processes makes environmental,[1] occupational,[2,3] and consumer exposure inevitable.[4,5] Nano enabled technologies are currently in use for various biomedical applications ranging from preventing the transmission of infectious diseases[6,7] to theranostic applications.[8] Nanoparticle mediated therapies have been introduced which can either enhance current diagnostic methods like MRI[9] and X-rays[10] or introduce new methods, such as photo acoustic tomography (PAT).[11]

Both the potential adverse health effects and the efficacy of theranostics are directly related to the nanoparticle–cell interactions and particle uptake from cells.[12] There is a plethora of published literature documenting the ability of ENPs to penetrate biological barriers and initiate a cascade of events, possibly leading to adverse health effects.[13]

It is also recognized that when nanoparticles enter physiological media, there is an instant formation of a protein coating, widely known as the protein corona.[14] The protein corona dictates to a great degree the behavior and the fate of the nanoparticles in biological systems:[15] it influences their agglomeration potential,[16] the nanoparticle adhesion to the cell membrane,[17] and potential cell-uptake and possible toxicity.[18] Due to the importance of the corona in the nanoparticle–cell interactions, many studies have focused on the identification of (a) parameters influencing the adsorption of proteins on the surface of nanoparticles in various physiological fluids[19] and (b) the role of the corona on the nanoparticle cell uptake.[20] Although these studies aim to investigate the nanoparticle–cell interactions, they do so indirectly by observing secondary features such as the cell adhesion/viability, morphology, metabolic activity, oxidative stress, and particle uptake, which are later related to nanoparticle properties such as size, shape, and surface chemistry/modifications.[21] Among them, the most commonly used metric is the quantification of particle uptake.[22,23]

Currently the leading method for the nanoparticle uptake quantification is the flow cytometry, which requires fluorescence ENPs.[24] However, only a limited number of industry

Special Issue: Sustainable Nanotechnology 2013

Received: March 4, 2014
Revised: June 8, 2014
Published: June 10, 2014

 © 2014 American Chemical Society 

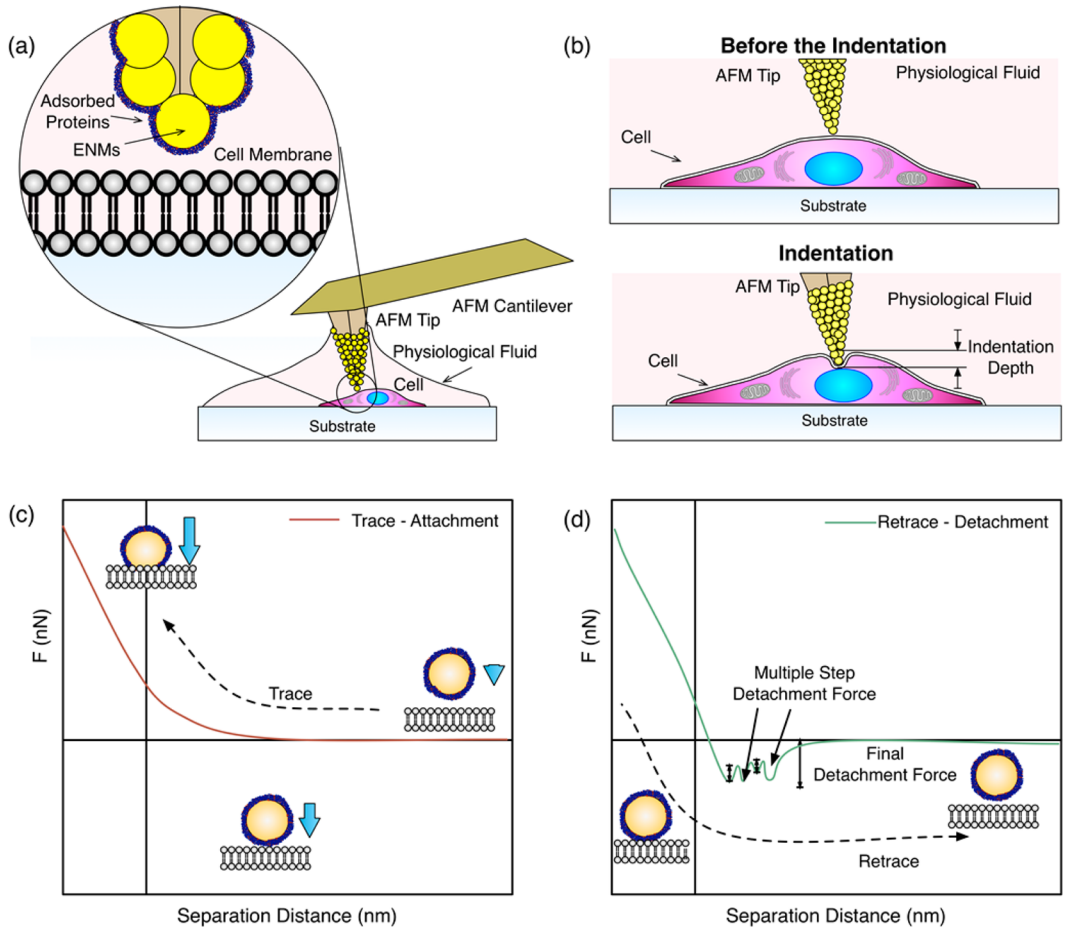


**Figure 1.** Illustration presenting the utilized research strategy. (a) Cell adhered to a substrate and a modified tip coming in contact with it. (b) Process of approaching the cell. (c) Trace force curve. (d) Typical force curve during retrace with the various parameters highlighted.

relevant ENPs possess intrinsic fluorescent properties and possible ENP surface modification with fluorescent dyes may alter the chemistry and affect the nanoparticle−cell interactions.[25] In an alternative approach, Wang et al. used the plasmonic properties of gold nanoparticles to study the intracellular localization of nanoparticles and recreate a three-dimensional mapping of their distribution,[26] which again is limited to small number of ENPs with intrinsic particle properties. Other researchers have used more conventional methods like ICP-MS to quantify the nanoparticle uptake.[27] James et al. used a very sophisticated method employing X-ray fluorescence microscopy to map ZnO particles distribution in THP-1 cells.[28] Recently, there have been attempts to utilize molecular dynamic simulations to investigate these interactions.[12] Although insightful, there are still inherent limitations of this approach including the finite number of atoms that can by added to the simulations and the inability to accurately simulate an entire cell. In summary, although all these aforementioned methods can provide some information on nanoparticle−cell interactions, they have major drawbacks: (a) they do not provide a direct quantification of the nanoparticle−cell interactions; (b) they depend on intrinsic particle properties (e.g., fluorescence, plasmonic resonance, etc.) which limits their applicability to only a few particle systems; and (c) they require highly specialized equipment.

It is evident that there is a lack of a methodology that is independent of the particle properties, cell type, and media that can directly measure the nanoparticle−cell interactions. We recently developed a methodology that allows for the direct measurement of nanoparticle−nanoparticle interactions using atomic force microscopy (AFM).[29] AFM is a state-of-the-art surface sensitive technique that has the ability to characterize in real time the interaction forces on a molecular level. While it has been used extensively in material science for imaging[30] and atomic force measurements,[31] only recently has the AFM been employed for understanding the nanoparticle-to-nanoparticle interactions in physiologic fluids.[32] The high reproducibility of the method in terms of preparation of ENP coated AFM tips and atomic force measurements was showcased in our recently published study by Pyrgiotakis et al.[29] It was also shown in this study that the agglomeration potential of $CeO_2$ nanoparticles in water was inversely proportional to their primary particle diameter, but for $Fe_2O_3$ nanoparticles, that potential is independent of primary particle diameter in these media. In RPMI (Roswell Park Memorial Institute Medium no. 1640) + 10% Fetal Bovine Serum (FBS), the corona thickness and dispersibility of the $CeO_2$ is independent of PP diameter while, for $Fe_2O_3$, the corona thickness and dispersibility were inversely proportional to primary particle (PP) diameter.

**Research Strategy.** In this companion study, our recently developed AFM platform was utilized to investigate nanoparticle−cell interactions in two relevant physiological media.[29] To the best of our knowledge, this is one of the first systematic studies to determine in real time the nanoparticle−cell interactions and atomic force profiles and link them to nanoparticle properties and biological media using AFM.

Figure 1a describes the overall research strategy. Industry relevant ENPs of controlled size were synthesized in house using the FSP based Harvard Versatile Engineering Nanomaterials Generation System (Harvard VENGES) system[33−35] and were attached on the surface AFM tips, as described in detail in the Materials and Methods section.[29] The interaction force between the ENP functionalized tips and the cells was measured. It is worth noting that FSP made ENPs are highly relevant as they account for 90% by volume of ENPs currently on the market.[36] Typical examples of FSP made ENPs are, among others, carbon black, pigmentary titania, and fumed silica, as well as other novel metal and metal oxide ENPs currently in use as catalysts, gas sensors, biomaterials, and even nutritional products.[37]

Two ENP systems were used as test materials in the study, $CeO_2$ and $Fe_2O_3$. These ENPs were synthesized in two different sizes, small (S) and large (L), and more specifically, approximately 5 and 50 nm for $CeO_2$ and 10 and 100 nm for $Fe_2O_3$. Both ENPs are extensively used in many applications. Cerium oxide is employed in many industrial and commercial applications such as a catalyst,[38] additive in fuels,[39] oxygen storage in fuel cells,[40] pigment in cosmetics,[41] and abrasive medium in chemical mechanical polishing (CMP).[42] Recent toxicological evidence suggests that in the nanoparticle form there might be adverse health effects[35] and environmental implications.[43] Iron oxide is widely utilized as pigment[44] and has attracted considerable attention due to its promising potential in biomedical applications for its superparamagnetic properties[11] and its use in nutritional[45] applications. In addition both ENPs have also been investigated in our recently published nanoparticle−nanoparticle interactions AFM study.[29]

As test cells, the A549 cell line (lung epithelia cells) were used. Epithelial cells constitute the first line of defense against ENPs in the lung. RPMI 1640 (Roswell Park Memorial Institute formulation 1640) and RPMI containing 10% Fetal Bovine Serum (FBS) were used as biological media in the study. The aforementioned media are commonly employed in the preparation of nanoparticle suspensions in toxicological studies[13,16]

During a typical AFM force measurement, the interaction between the ENP modified tips and the cells is divided in two subsequent modes, trace and retrace modes. "Trace mode" is referred to the approach of the tip to the cell, while "retrace mode" is referred to the retraction of the tip away of the cell.[46] The atomic force is obtained as a function of the distance between AFM tip and cell surface for both modes. Additionally, the AFM allows the regulation of the contact time (dwell time) of the tip with the cell surface (see Figure 1b for more details). During the approach of the AFM tip toward the cell surface (trace mode), the nanoparticle surface (with or without a protein corona) and the various molecules of the cell membrane (lipids, proteins, receptors etc.) will be compressed as they come in contact. Further pressing the tip on the cell will result in the tip indenting the cell and deforming the shape (Figure 1b). This is an elastic deformation of the cell wall will complete recover upon stopping the application of the force.[47] At some point, the compression will stop, and the tip cantilever will start bending, resulting in a force which is linearly increasing with the distance from cell surface (Figure 1c).[29] During the retrace, different force curve is observed as several phenomena occur: (a) multiple small detachment forces shown as a "see-saw" pattern in the atomic force curve and (b) a final detachment force, which is distinctly larger than the small detachment forces and indicates the complete detachment of the tip from the cell surface (Figure 1d). The typical see-saw pattern is characteristic of the multiple events of adhesive bonds between the ENPs and the cell surface, breaking sequentially.[48] During the retrace there are three important parameters that define the ENP-cell interactions: (a) The average magnitude of the force to break these individual bonds which is defined as *atomic force per bond* (AFB); (b) the number of these breaking bonds (*number of bonds* (NB); and (3) the *detachment force* (DF) which is defined as the final larger single event force for the complete detachment of the ENPs. These three aforementioned parameters were used as metrics for the data analysis in this study.

## MATERIALS AND METHODS

The utilized AFM methodology has been fully described and characterized in our previous publication.[29] In brief, the ENP synthesis and characterization, the AFM tip preparation, the cell substrate preparation, and the force acquisition and analysis were performed as follows:

**Synthesis of ENPs.** The nanoparticles were synthesized using Harvard VENGES,[33−35] which is based on flame spray pyrolysis (FSP).[49] The exact procedure is described in detail in our previous publication.[29] Flame aerosol technology accounts for more than 90% of the total volume of all nanomaterials produced in the gas-phase worldwide.[50] Among the advantages of this method is its precise control of the nanoparticle properties (i.e., composition, dimensions, shape, etc.), the high yield (g/h), the ease of scaling, and the reproducibility with regard to nanoparticle properties.[37]

In brief, during the FSP synthesis, a precursor solution, which contains dissolved organometallic compounds in a high enthalpy solvent, is pumped through a stainless-steel capillary tube at a controlled flow rate. Oxygen flow disperses the liquid precursor solution into fine droplets, which in turn are combusted by a small pilot flame. This results in the full conversion of the liquid precursor's organic constituents into metal oxide nanoparticles. The nanoparticle diameter is fully controlled by the operational parameters, and the results are consistent and reproducible.[49] The nanoparticles are collected on a water-cooled glass fiber filter (Whatmann, 25.5 cm Ø) for off-line characterization and further use.

**ENP Dispersion Preparation.** ENP dispersion was used for the AFM tip modification as described in detail by Pyrgiotakis et al.[29] The ENP dispersions in deionized water (18.1 MΩ/cm) were prepared according to the protocol developed by Cohen et al.,[16] that includes calibration of sonication equipment to ensure accurate application of delivered sonication energy (DSE) in joules per millileter in order to break agglomerates that might have formed.[51] This method is currently standardized and widely used for preparation of nanoparticles for toxicological studies.[13,16,52] According to the protocol, in order to achieve stable nanoparticle suspensions over time, the delivered sonication energy (DSE) should exceed a critical value ($DSE_{cr}$). The $DSE_{cr}$ for various ENPs has been previously experimentally determined, and the values varied from 161 to 242 J/mL.[16] The required sonication was done with a Branson Sonifier S-450A (Branson Ultrasonics, Danbury, CT, USA) fitted with a 3 in. cup.

**ENP Characterization.** The ENPs were characterized by transmission electron microscopy (TEM) regarding their morphology and by X-ray diffraction (XRD) regarding their crystal structure and size. BET $N_2$-adsorption was used to measure their surface area and the equivalent diameter. In more detail:

*TEM.* ENP dispersions were prepared as described before. After sonication, the nanoparticle suspension was diluted down to 100 μg/mL. TEM grids (Ted Pella Inc., Redding, CA) were submerged in the solution and were let to dry. The particles were imaged with the Libra 120 (Carl, Zeiss Oberkochen, Germany).

*XRD.* The X-ray diffraction pattern was measured from 2θ 15−70° with a Bruker AXS D8 Advance (Bruker, Karlsruhe, Germany). The

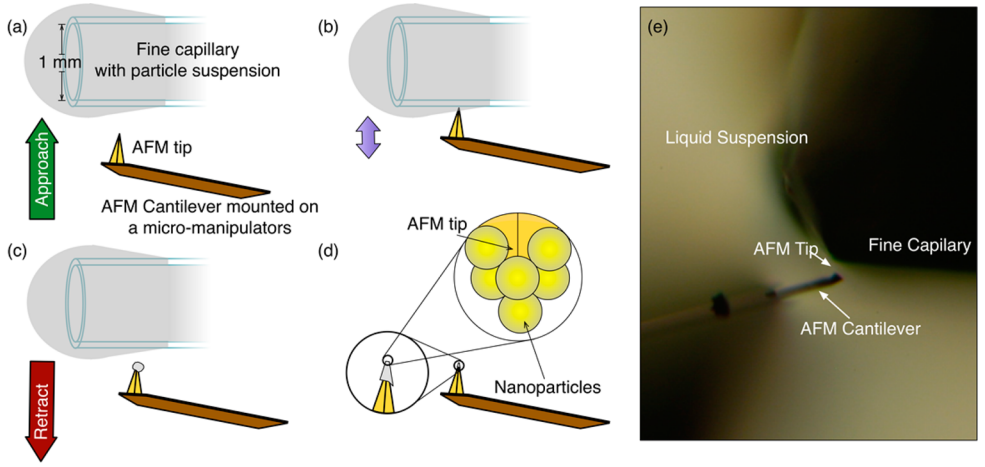


**Figure 2.** Method for tip preparations. (a) The tips are coated with the creation of a fine droplet on the edge of a fine capillary. (b) The tip is brought in contact with the created droplet and is dunked several times. (c) A micro sized droplet is formed at the edge of the tip. (d) The droplet is left to dry to create a small particle aggregate. (e) A photograph that depicts the process with the key elements illustrated.

analysis of the diffraction spectrum was done with the instrument software (Topas 4 software, Bruker, Karlsruhe, Germany) using a Rietveld method to determine the nanoparticle phase and crystalline size.

*Specific Surface Area.* BET $N_2$-adsorption of the nanoparticles allowed for the determination of the specific surface area. Approximately 100−200 mg of the nanoparticle was flushed with a $N_2$ gas at 150 °C for >1 h with the Flow Prep 060 (Micromeritics, Norcross, GA). The specific surface area was measured with TriStar (Micromeritics, Norcross, GA).

**Cell Culture and Cell Substrate Preparation.** For this set of experiments, the A549 lung epithelia cells were used (ATCC; cell line number CCL-185). They were selected due to the relevance to nanoparticle respiratory exposures and their resilience to the AFM conditions.

The growth media is made of 90% RPMI-1640 with L-glutamine (from Cellgro; cat. no.: 25-053-CI) and 10% Fetal Bovine Serum (four times filtered through 0.1 $\mu$m filter, from Hyclone; cat. no.: SH30070.03). The cells were cultured and plated according to the suggested ATCC protocols.[53] For all the experiments the cells were used between passages 5−10.

For these experiments, the cells were seeded on a on cover glass bottom sterile culture dish (70674-02, Electron Microscopy Sciences, Hatfield, PA) at approximately $5 \times 10^4$ cells by seeding 100 $\mu$L of cell suspension to cover the glass bottom of the culture dish. The substrates were placed in the incubator for 45 min, sufficient time for the cells to attach on the glass bottom of the culture dish. Following attachment the cells were washed and 1 mL of growth media was added and the cells were incubated at 37 °C and 5% $CO_2$ for a minimum of 24h before conducting AFM measurements. Prior to the usage of the AFM the media was removed, the cells were rinsed with PBS (Phosphate Buffer Saline) and the appropriate media was added.

**Modification of the AFM Tips.** *AFM Tip Selection.* It is critical for the AFM cantilever to yield before the tip punctures the cell. In order to ensure that, the AFM tips with small spring constants should be used (0.1 N/m). The tip type was optimized by trial and error. Several types of tips were tried, and the tip producing consistent and reproducible results was selected. It is worth noting that long cantilevers, although have small spring constant, which is appropriate for this study, are hard to functionalize as they are very wobbly. The selected tip was the BioLever Mini (Olympus BL-AC40TS, Asylum Research, Santa Clara, CA).

*Attachment of ENPs on AFM Tips.* The ENPs were ex situ attached on the tips from aqueous suspensions according to the method developed by Pyrgiotakis et al.[29,54]

The ENPs were attached on the AFM cantilever tips (BL-AC40TS) with a fine coordination of Leica micromanipulators (Micro-manipulator L, Leica Microsystems, Buffalo Grove, IL) under an upright microscope (Leica DMIRB, Leica Microsystems, Buffalo Grove, IL) with a 20× magnification lens. The AFM cantilever tip was brought into the vicinity of a flint glass capillary tube (VWR, Radnor, PA) previously filled with the desired nanoparticle aqueous dispersion. A small dispersion droplet was ejected from the capillary and carefully allowed to circulate the first 5 mm of the outside cylindrical surface of the capillary tip for about 2 min in order to evenly wet the capillary front. The tip was then slowly brought into contact with the remaining dispersion for 15−30 touch intervals. Subsequently, the AFM tips were allowed to dry at ambient room condition, and then they were rinsed with deionized water. Figure 2 summarizes this procedure. It is very crucial to fully coat the tip to ensure that only particles and not "bare" sides of the AFM tip come in contact with the cell surface. This was verified with SEM imaging of the tips after the nanoparticle attachment.

**Force Measurements Using AFM.** *AFM Preparation and Setup.* All the measurements were conducted with the Asylum MFP-3D AFM System (Asylum Research, Santa Barbara, CA) sitting on a TS-150 vibration isolation table (Asylum Research, Santa Barbara, CA) and enclosed in AEK 2002 acoustic isolation enclosure (Asylum Research, Santa Barbara, CA). The AFM was positioned on top of an inverted Olympus IX81 optical microscope. A photograph of the experimental setup highlighting the various components is supplied in Figure S1 (Supporting Information).

The cell substrate was fixed with two glass slides (one in each side) with Crystalbond 509 adhesive (Ted Pella Inc., Redding, CA) in order to allow room for the microscope lens. No additional instruments were required for the liquid measurements as they were executed by forming a liquid meniscus between the AFM tip holder and the substrate (Figure 1a). The force curves were obtained in two different environments: RPMI and RPMI+10% FBS. For all the cases, the cell substrate and the AFM tips were left in the utilized media for 30 min prior to use. This ensures that the system reaches equilibrium and sufficient time is given for the protein corona to be formed on the nanoparticle surface.

For each experiment, a different nanoparticle functionalized tip and a different cell substrate was used. The cell substrate was used for a maximum of 2 h, which is proven not to affect the cell function.[55,56]

*AFM Tip Spring Constant Measurement.* The spring constant and the resonance frequency of the AFM tips were measured before and after the nanoparticles attachment to account for the added mass of the particles and the corresponding change to the resonance frequency. It was experimentally determined in air over a clean glass surface according to the standardized protocol developed by Torii et al.[57]

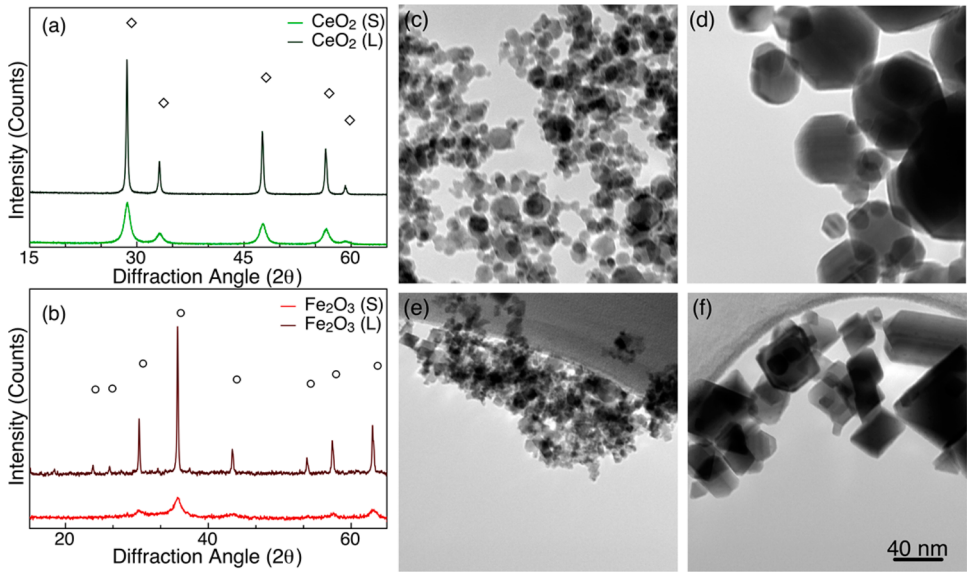


**Figure 3.** Structural characterization of the utilized nanoparticle system. XRD patterns for the (a) $CeO_2$ and $Fe_2O_3$ nanoparticles. TEM images of the (c) $Fe_2O_3$(S), (d) $Fe_2O_3$(L), (e) $CeO_2$(S), and (f) $CeO_2$(L).

*Force Measurement Protocol.* For each nanoparticle−cell interaction, two to five sets of tips and cells were used. For each measurement session, 10−30 randomly selected cells (including cells in a monolayer and isolated cells) were investigated during each session. The cantilever tip was aligned on various locations over the cells by using the built-in inverted microscope. For each cell, one to five consecutive extension/retraction movements were conducted per cell at a speed of 100 nm/s. For multiple measurements per cell, different touchdown locations were selected. The forces acting between the cell and the modified tip were measured by bring the tip into contact at 1 nN. This ensures that for all experiments the tip will push the cell surface down (indentation) for approximately 400 nm. The smaller the size of the particles attached on the AFM tip, the more particles might come in contact with cell membrane. Unfortunately, it is currently not possible to control and measure the number of particles coming in contact with the cell surface. Instead, the depth of the indentation was kept constant at approximately 400 nm for all experiments, regardless of the size of the particles.

Preliminary data showed that the 1 nN does not impact the cell. Our data show that an unfunctionalized tip could puncture the cells for forces greater than 20 nN.

The tip was left in contact (dwell time) for either 30 or 180 s while the feedback maintained a constant force of 1 nN between tip and cell.

*Force Measurement Analysis.* The AFM measures the force as a function of the tip displacement and not directly as a function of the surface tip distance. Instead each curve was individually analyzed and the values of DF, NB, and AFB were derived. In total approximately 150−200 force curves were analyzed for each case.

*Statistics.* Once the curves were analyzed regarding the NB, DF, and FPB parameters, the values of each parameter were averaged, and the average values were used with standard deviation shown as the error bar. The comparison between values was based on ANOVA and the *p*-value calculated with Prism by GraphPad. ANOVA was preformed in pairs of the examined values. A Bonferroni test was used to estimate the confidence intervals and significance. Comparison between two parameters that resulted in $p$-value < 0.05 was considered statistically significant.

## RESULTS AND DISCUSSION

**Particle Synthesis and Characterization.** These particular ENPs have been already rigorously characterized in our previous publication.[29] The $CeO_2$ and $Fe_2O_3$ nanoparticles were synthesized in two distinctly different primary diameters of 5−10 and 50−100 nm. Figure 3 shows collectively the structural characterization of $CeO_2$ (Figure 3a) and $Fe_2O_3$ (Figure 3b) nanoparticles for both diameters. Figure 3c−f shows the TEM images of the same particles. Table S2 (Supporting Information) summarizes the results of the particle characterization including the diameter based on the XRD patterns (Rietveld analysis) and the Brunauer−Emmett−Teller (BET) $N_2$ adsorption specific surface area.

As it is evident from the XRD patterns, both $CeO_2$ and $Fe_2O_3$ are crystalline. More specifically, the $CeO_2$ nanoparticles have the characteristic cubic ($CaF_2$ structural type), in agreement with literature,[49] and the $Fe_2O_3$ nanoparticles are in gamma phase, also in agreement with FSP literature.[58] In addition, the TEM showcase the characteristic hexagonal form of the $Fe_2O_3$ particles[59] and the rhombohedral shape of the $CeO_2$ particles.[49] The desired diameter variation is confirmed by both the XRD patterns and TEM images (Table S2, Supporting Information). It is worth noting that there is a nearly self-preserving diameter, as it is true for all flame generated materials.[36]

The DLS characterization was extensively described in our previous publication[29] and showed that all particles suspensions follow unimodal particle distributions, fairly monodispersed with the PDIs ranging from 0.261 to 0.674 in both media, which is in accordance with previous publications.[13,16,60]

**AFM Tip Preparation and Characterization.** Figure 4a−d shows an SEM image of the AFM tips modified with the $CeO_2$(L), $CeO_2$(S), $Fe_2O_3$(L), and $Fe_2O_3$(S) nanoparticles, respectively. In both cases, it is evident that the tips are coated with the nanoparticles with a single nanoparticle protruding. In our previous publication, we examined the stability of the tips by successively imaging them with SEM after 200 measurements in air, 200 measurements water, 200 measurements RPMI, and 200 measurements RPMI+10% FBS.[29] Examination of the tips before and after each measurement in this study also showed that the nanoparticles remain in place after each measurement. Overall, our current data showed that the utilized method results in nanoparticles very well adhered on AFM tips.[29]


dx.doi.org/10.1021/sc500152g | ACS Sustainable Chem. Eng. 2014, 2, 1681−1690

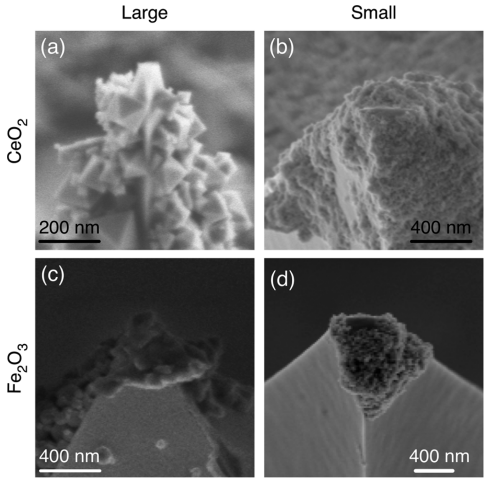


**Figure 4.** Characteristic images of the modified AFM tips with (a) $CeO_2$(L), (b) $CeO_2$(S), (c) $Fe_2O_3$(L), and (d) $Fe_2O_3$(S).

**Atomic Force Profiles: Nanoparticle−Cell Interactions.** Supporting Information Figure S2 shows a typical force curve during the cell approach (trace mode) and cell retraction (retrace mode). The three important parameters/metrics that define the ENP−cell interactions, namely, the detachment force (DF), the atomic force per bond (AFB), and the number of bonds (NB) are illustrated in the figure as well. The number of bonds usually follows a normal distribution as shown in Figure S2b.

The results of this analysis are summarized in Figure 5 for both RPMI+10% FBS and RPMI media for a 30 s dwell time. Figure 5a, b, and c show the DF, NB, and AFB metrics, respectively, for both the $CeO_2$ and $Fe_2O_3$. Figure 5d−f shows the same parameters for the 180 s dwell time. The related *p*-values are listed in Supporting Information Tables S3−S10.

*Role of Biological Media.* DF appears to be greater for the case of pure RPMI compared to RPMI+10%FBS regardless of the material or the size of the nanoparticles, with only exception to the observation the small $CeO_2$, where the *p*-value is not showing statistical significant difference (Figure 5a). In the case of the 30 s dwell time, the DF values are significantly greater as compared to the RPMI+10%FBS for all the cases with the exception of the small $CeO_2$ nanoparticles, where the difference is not significant due to the relative large statistical error. These observations indicate that the cells have a stronger affinity to the nanoparticles in the absence of serum proteins (no protein corona). These results are in good agreement with the literature. It was shown in previous published studies that protein corona plays a significant role on the cellular uptake of ENPs.[18] Tedja et al. showed that the serum proteins result in reduced titania nanoparticle uptake.[61] Similarly, Johnstone et al. showed that the surface associated serum proteins inhibit the particle uptake of various polymer nanoparticles.[62]

Moreover, the number of bonds forming between the nanoparticles and the cell surface (Figure 5b) is also significantly greater for the case of pure RPMI, as compared to the nanoparticles in RPMI+10% FBS, with exception of the case of the small $Fe_2O_3$ nanoparticles that the observed difference is within the experimental error. (See related *p*-values in Supporting Information Table S10). This is in agreement that with our previous hypothesis, stating that the nanoparticles in the absence of serum have higher affinity toward the cells. The nanoparticle surface without the protein corona has more binding sites available from the various constituents of the cell to attach, and therefore the number of bonds is significantly higher.[61] The larger particles have higher surface area per particle. They offer more binding sites, which may result to greater DF values.

The corona formation and characteristics are particle/media dependent and play an important role in nanoparticle cell uptake and biointeractions in general.[13,16] In the future, we plan to expand the investigation and characterize the protein coronas on the nanoparticle systems used here in order to better understand the link between corona characteristics and AFM measured interactions.

*Role of ENP Size.* It is also interesting to examine the effect of the ENP size on the magnitude of the detachment force (DF). For the $CeO_2$ nanoparticles in RPMI media, the nanoparticle size has a significant effect on DF value, while in the case of RPMI+10% FBS, the nanoparticles size does not have a significant effect. However, for the of the $Fe_2O_3$ nanoparticles, the smaller size results in larger DF, but the difference is not as strong as for the case of the $CeO_2$ nanoparticles. This differences observed in the material dependency might be explained by the differences previously observed in corona properties.[29] As shown in our previously published companion AFM study on nanoparticle−nanoparticle interactions,[29] the repulsive layer thickness (RLT, an estimate of the protein corona thickness) of the $Fe_2O_3$ nanoparticles decreased with the size, a clear indication that the corona properties were size dependent. These findings reflect differences on the size of the corona and do not necessarily reflect differences in corona composition. It is well documented that the corona composition depends both on the particle size and surface properties.[63]

In the case of the pure RPMI and the absence of protein corona, the adhesion of both $CeO_2$ and $Fe_2O_3$ nanoparticles to cells show stronger dependence on the particle size as indicated by the DF. More specifically, the larger $CeO_2$ nanoparticles have an approximate 2-fold DF compared to the smaller $CeO_2$ nanoparticles. Similar findings were found for the $Fe_2O_3$ nanoparticles although the size dependency was found to be less prominent.

Finally, in the case of RPMI, the NB was found to depend on the particle size (Figure 5b and e). Generally larger nanoparticles displayed a higher NB value. Larger nanoparticles offer more absolute surface per single particle and therefore more binding sites.[64] It is worth noting that, in RPMI, there was no significant difference observed.

*Role of Dwell Time.* Figure 5d, e, and f shows the same parameters (DF, NB, AFB, respectively), for the case of the larger contact time (180 s). The calculated *p*-values are summarized in Supporting Information Table S6. The general trends observed for the DF in the case of 30 s dwell time seem to remain the same for this case. The $CeO_2$ nanoparticles have stronger DF values as compared to the $Fe_2O_3$ ones regardless of the media. It should also be noted that the various differences between RPMI and RPMI+10% FBS seem to have been reduced for the longer dwell time. It is also evident that for the $CeO_2$ nanoparticles the longer dwell time results in stronger DF as compared to the case of 30 s, while the opposite is observed for the $Fe_2O_3$.

The direct comparison of the DF parameter for the dwell times of 30 and 180 s shows that in pure RPMI the DF at 180 s appears to be greater compared to the 30 s for the $CeO_2$ nanoparticles. The $Fe_2O_3$ nanoparticles follow the opposite

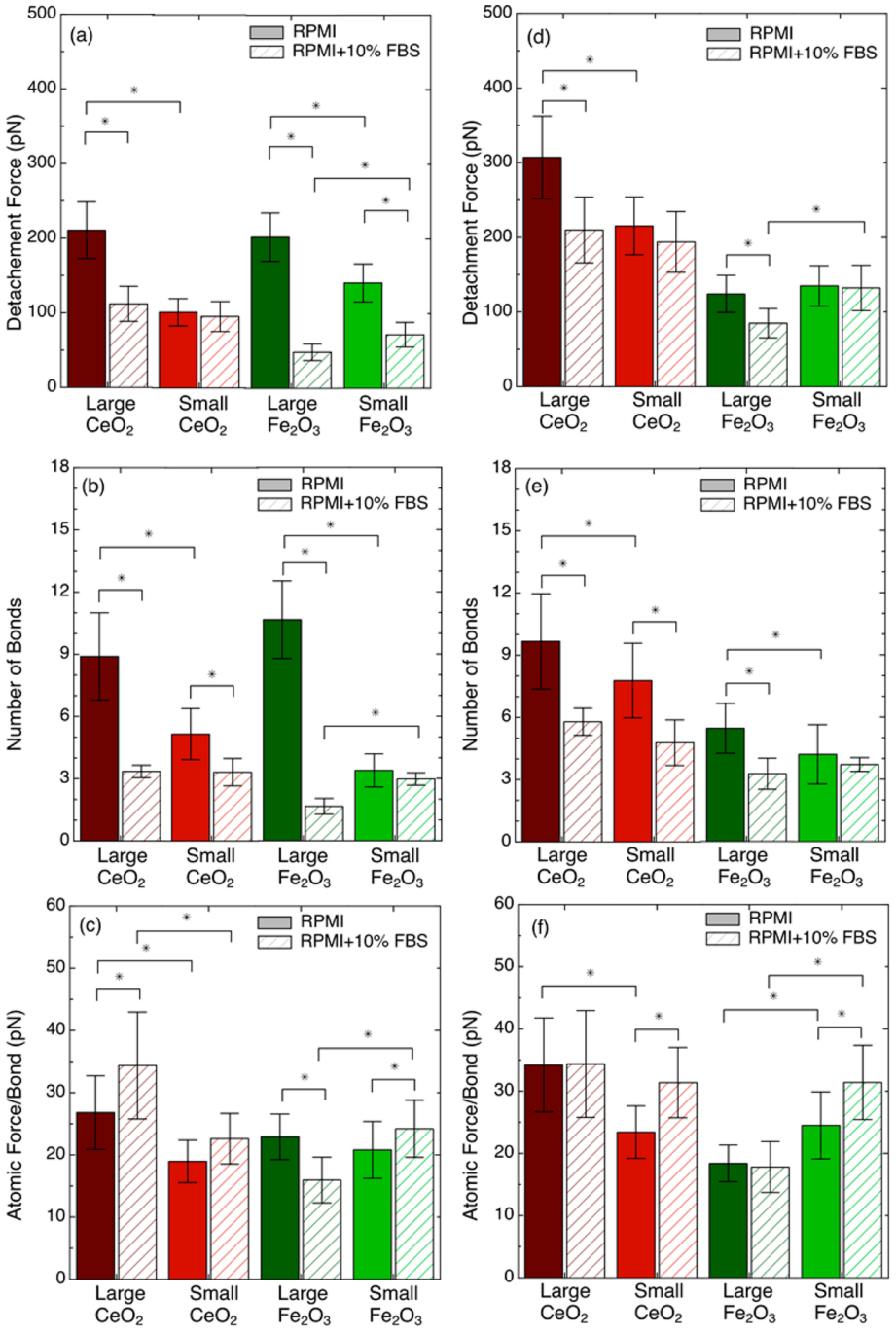


**Figure 5.** Various metrics of the nanoparticle−cell interactions in RPMI and RPMI+10% FBS for 30 s dwell times: (a) detachment force, (b) number of bonds, and (c) atomic force per bond. The symbol * indicate $p < 0.05$. The various metrics of the nanoparticle−cell interactions in RPMI and RPMI+10%FBS for 180 s dwell times: (d) detachment force, (e) number of bonds, and (f) atomic force per bond. The symbols * indicate $p < 0.05$.

trend with DF value to be either small or not changing between the dwell times ($p$-values are summarized in Supporting Information Table S9).

For the case of RPMI+10% FBS and 180 s dwell time, DF values are consistently greater as compared to the 30 s dwell time regardless of the material type and size. These observations are in agreement with other published studies indicating the dependency on interaction time of the protein adsorption on the nanoparticle surface.[65,66] Similarly, these findings are also in agreement with computer simulations studying the nanoparticle cell interactions.[67] It was previously shown that longer dwell time (time scale of minutes) brings the adsorption dynamics closer to equilibrium. Here this is causing the difference in DF between the RPMI and the RPMI+10% FBS to be reduced.[68]

Moreover, similar trends are observed for the NB parameter. More specifically, the small $CeO_2$ nanoparticles have a significant higher NB while the small $Fe_2O_3$ nanoparticles do not show significant differences between the two dwell times. For the large $Fe_2O_3$ in RPMI, the NB value is reduced by 50% while for the small $Fe_2O_3$ it remains unchanged (see $p$-values in Supporting Information Table S10). It is worth noting that the


dx.doi.org/10.1021/sc500152g | ACS Sustainable Chem. Eng. 2014, 2, 1681−1690

trends are consistent with the observations regarding the DF In addition, the differences in terms of NB values between the RPMI and RPMI+10% FBS seem to decrease for the longer dwell time. Again, this might be explained on the basis of the equilibrium of the protein adsorption that is achieved at longer dwell times.[68]

*Atomic Force Bond (AFB).* The magnitude of the AFB was found to be independent of media, dwell time, size of ENP, and the material. More specifically, AFB in RPMI does not show any dependency with either the size or the material (Figure 5c and f). This is in agreement with literature describing interactions of various organic molecules with various substrates (fibrinogen on gold and mica surface).[69] Similarly, in the case of the RPMI+10% FBS, there is no significant difference of the AFB values either as a function of the nanoparticle size or the material. Further there is no statistically significant difference between the AFB in RPMI and the AFP in RPMI+10% FBS. The magnitude of these forces are in agreement with similar studies by Ikai et al. describing the interaction of protein (conA protein) and bacteria (yeast cells *Saccharomyces cerevisiae*).[48]

*Overall Nanoparticle Affinity to the Cells.* Evaluating the results collectively, it is clear that both ENPs used in this study have an affinity toward the A549 cells. In the case of the in RPMI, the adhesion is governed by the size with the larger nanoparticles exhibiting higher affinity. In the case of the RPMI +10% FBS the adhesion is mainly governed by the material with the $CeO_2$ to exhibit larger DF, regardless of the size and the dwell time. Although quantification of the nanoparticle uptake is out of the scope of this manuscript, in numerous previously published studies, it has been demonstrate that A549 can uptake both $CeO_2$ and $Fe_2O_3$ nanoparticles. Gass et al. showed that the $Fe_2O_3$ nanoparticles can be taken up by A549 cells and can lead to potential adverse effects.[70] Furthermore, $Fe_2O_3$ nanoparticles were shown to be uptaken by alveolar cells during inhalation and can cause adverse health effects. Sotiriou et al. also demonstrated with animal inhalation studies that $Fe_2O_3$ nanoparticles can cross the air−blood barrier and can cause oxidative stress in the lung and the heart of the exposed animals.[34] Similarly, the $CeO_2$ nanoparticles were found to be taken up by cells in in vitro[35,70] and in vivo studies.[35] This has been documented by Demokritou at al. where it was shown that $CeO_2$ ENPs were taken up by lung epithelia cells after animal inhalation exposures.[35] These type of interactions depend on the particle properties, cells, and the media, and therefore, trends observed here cannot be generalized or even extrapolated to other cell types or particles. Further research is required to be able to derive more generalized conclusions.

## CONCLUSIONS

This study is one of the first attempts to assess in a systematic manner the role of the protein corona to the nanoparticle−cell interactions in relevant physiological media using atomic force microscopy. The AFM platform enables a real time direct measurement of the ENP−cell interactions. Results from this study highlight the important role of protein corona in the particle−cell interactions as indicated by the higher nanoparticle−cell interaction force in the case of the presence of serum proteins in the biological media. This AFM approach provides an additional layer of information on atomic force interactions, which can be valuable in the quest of understanding the complex nanobio interactions.

In the future, we plan to use the developed AFM platform to investigate the forces between nanoparticles and various cell lines under conditions where certain nanoparticle internalization mechanisms have been blocked. This will allow the investigation of the specific role of the nanoparticle properties in the internalization mechanisms.

## ASSOCIATED CONTENT

### Supporting Information

Summary of the synthesis parameters, particle characterization, a typical AFM force curve, and the *p*-values of the statistical analysis. This material is available free of charge via the Internet at http://pubs.acs.org/.

## AUTHOR INFORMATION

### Corresponding Author

*Tel.: 617 432 3481. Mailing Address: Bldg 1, Rm 1310B, 665 Huntington Avenue, Boston MA 02115.

### Notes

The authors declare no competing financial interest.

## ACKNOWLEDGMENTS

The authors would like to acknowledge funding for this study from the Center for Nanotechnology and Nanotoxicology at the Harvard School of Public Health, the HSPH Career Incubator Fund, NSF (grant ID no. 1235806), NIH (grant ID no. P30ES000002). The authors would also like to acknowledge Dr. Sotiris Pratsinis, (ETH Zurich) for his valuable input. This work was performed in part at the Harvard Center for Nanoscale Systems (CNS), a member of the National Nanotechnology Infrastructure Network (NNIN), which is supported by the National Science Foundation under NSF award no. ECS-0335765.

## REFERENCES

(1) Gao, W.; Wang, J. The Environmental Impact of Micro/Nanomachines: A Review. *ACS Nano* **2014**, *8*, 3170−3180.

(2) Dhimiter, B.; Martin, J.; Santeufemio, C.; Sun, Q.; Lee Bunker, K.; Shafer, M.; Demokritou, P. Physicochemical and morphological characterisation of nanoparticles from photocopiers: implications for environmental health. *Nanotoxicology* **2012**, *7*, 989−1003.

(3) Pirela, S.; Pyrgiotakis, G.; Dhimiter, B.; Treye, T.; Castranova, V.; Demokritou, P. Development and characterization of an exposure platform suitable for physico-chemical, morphological and toxicological characterization of Printer Emitted Particles (PEPs). *Inhal. Toxicol.* **2014**, *26* (7), 400−408.

(4) Philbert, M. A.; Alexeeff, G. V.; Bahadori, T.; Balbus, J. M.; Bawendi, M. G.; Biswas, P.; Colvin, V.; Klaine, S. J.; Maynard, A. D.; Monteiro-Riviere, N. A.; et al. *Review of Federal Strategy for Nanotechnology-Related Enviromental, Health, and Safety Research*; The National Academic Press: Washington, DC, 2008; pp 1−131.

(5) Sotiriou, G.; Watson, C.; Murdaugh, K.; Darrah, T. H.; Pyrgriotakis, G.; Elder, A.; Brain, J.; Demokritou, P. Engineering safer-by-design, transparent, silica-coated ZnO nanorods with reduced DNA damage potential. *Environ. Sci.: Nano* **2014**, *1*, 144−153.

(6) Pyrgiotakis, G.; McDevitt, J.; Bordini, A.; Diaz, E.; Molina, R.; Watson, C.; DeLoid, G.; Lenard, S.; Fix, N.; Mizuyama, Y.; et al. A chemical free, nanotechnology-based method for airborne bacterial inactivation using engineered water nanostructures. *Environ. Sci.: Nano* **2014**, *1*, 15−26.

(7) Pyrgiotakis, G.; McDevitt, J.; Yamauchi, T.; Demokritou, P. A novel method for bacteria inactivation using Engineered Water Nanostructures. *J. Nanopart. Res.* **2012**, *14*, 1027−1038.

(8) Grobmyer, S. R.; Morse, D. L.; Fletcher, B.; Gutwein, L. G.; Sharma, P.; Krishna, V.; Frost, S. C.; Moudgil, B. M.; Brown, S. C. The

promise of nanotechnology for solving clinical problems in breast cancer. *J. Surg. Oncol.* **2011**, *103*, 317−325.
(9) Bu, L.; Xie, J.; Chen, K.; Huang, J.; Aguilar, Z. P.; Wang, A.; Sun, K. W.; Chua, M.-S.; So, S.; Cheng, Z.; et al. Assessment and comparison of magnetic nanoparticles as MRI contrast agents in a rodent model of human hepatocellular carcinoma. *Contrast Media Mol. Imaging* **2012**, *7*, 363−372.
(10) Jain, K. K. Advances in the field of nanooncology. *BMC Med.* **2010**, *8*, 83.
(11) Xi, L.; Grobmyer, S. R.; Zhou, G.; Qian, W.; Yang, L.; Jiang, H. Molecular photoacoustic tomography of breast cancer using receptor targeted magnetic iron oxide nanoparticles as contrast agents. *J. Biophotonics* **2014**, *7*, 401−409.
(12) Ding, H.-M.; Ma, Y.-Q. Controlling Cellular Uptake of Nanoparticles with pH-Sensitive Polymers. *Sci. Rep.* **2013**, *3*.
(13) Cohen, J. M.; Derk, R.; Wang, L.; Godleski, J.; Kobzik, L.; Brain, J.; Demokritou, P. Tracking translocation of industrially relevant engineered nanomaterials (ENMs) across alveolar epithelial monolayers in vitro. *Nanotoxicology* **2014**, 1−10.
(14) Faunce, T. A.; White, J.; Matthaei, K. I. Integrated research into the nanoparticle−protein corona: a new focus for safe, sustainable and equitable development of nanomedicines. *Nanomedicine* **2008**, *3*, 859−866.
(15) Lynch, I.; Salvati, A.; Dawson, K. A. Protein-nanoparticle interactions: What does the cell see? *Nat. Nanotechnol.* **2009**, *4*, 546−547.
(16) Cohen, J.; DeLoid, G.; Pyrgiotakis, G.; Demokritou, P. Interactions of engineered nanomaterials in physiological media and implications for in vitrodosimetry. *Nanotoxicology* **2012**, *7*, 417−431.
(17) Lesniak, A.; Salvati, A.; Santos-Martinez, M. J.; Radomski, M. W.; Dawson, K. A.; Åberg, C. Nanoparticle Adhesion to the Cell Membrane and Its Effect on Nanoparticle Uptake Efficiency. *J. Am. Chem. Soc.* **2013**, *135*, 1438−1444.
(18) Yan, Y.; Gause, K. T.; Kamphuis, M. M. J.; Ang, C.-S.; O'Brien-Simpson, N. M.; Lenzo, J. C.; Reynolds, E. C.; Nice, E. C.; Caruso, F. Differential Roles of the Protein Corona in the Cellular Uptake of Nanoporous Polymer Particles by Monocyte and Macrophage Cell Lines. *ACS Nano* **2013**, *7*, 10960−10970.
(19) Wasdo, S. C.; Juntunen, J.; Devarajan, H.; Sloan, K. B. A comparison of the fit of flux through hairless mouse skin from water data to three model equations. *Int. J. Pharm.* **2009**, *366*, 65−73.
(20) Nativo, P.; Prior, I. A.; Brust, M. Uptake and Intracellular Fate of Surface- Modified Gold Nanoparticles. *ACS Nano* **2008**, *2*, 1639−1644.
(21) AshaRani, P. V.; Low Kah Mun, G.; Hande, M. P.; Valiyaveettil, S. Cytotoxicity and genotoxicity of silver nanoparticles in human cells. *ACS Nano* **2009**, *3*, 279−290.
(22) Treuel, L.; Nienhaus, G. U. Toward a molecular understanding of nanoparticle−protein interactions. *Biophys Rev.* **2012**, *4*, 137−147.
(23) Treuel, L.; Jiang, X.; Nienhaus, G. U. New views on cellular uptake and trafficking of manufactured nanoparticles. *J. R. Soc. Interface* **2013**, *10*, 20120939−20120939.
(24) Ibuki, Y.; Toyooka, T. Nanoparticle Uptake Measured by Flow Cytometry. In *Methods in Molecular Biology*; Humana Press: Totowa, NJ, 2012; Vol. *926*, pp 157−166.
(25) Salvati, A.; Pitek, A. S.; Monopoli, M. P.; Prapainop, K.; Bombelli, F. B.; Hristov, D. R.; Kelly, P. M.; Aberg, C.; Mahon, E.; Dawson, K. A. Transferrin-functionalized nanoparticles lose their targeting capabilities when a biomolecule corona adsorbs on the surface. *Nat. Nanotechnol.* **2013**, *8*, 137−143.
(26) Wang, S.-H.; Lee, C.-W.; Chiou, A.; Wei, P.-K. Size-dependent endocytosis of gold nanoparticles studied by three-dimensional mapping of plasmonic scattering images. *J. Nanobiotechnol.* **2010**, *8*, 33.
(27) Chithrani, B. D.; Ghazani, A. A.; Chan, W. C. W. Determining the Size and Shape Dependence of Gold Nanoparticle Uptake into Mammalian Cells. *Nano Lett.* **2006**, *6*, 662−668.
(28) James, S. A.; Feltis, B. N.; de Jonge, M. D.; Sridhar, M.; Kimpton, J. A.; Altissimo, M.; Mayo, S.; Zheng, C.; Hastings, A.; Howard, D. L.; et al. Quantification of ZnO Nanoparticle Uptake, Distribution, and Dissolution within Individual Human Macrophages. *ACS Nano* **2013**, *7*, 10621−10635.
(29) Pyrgiotakis, G.; Blattmann, C. O.; Pratsinis, S.; Demokritou, P. Nanoparticle-nanoparticle interactions in biological media by atomic force microscopy. *Langmuir* **2013**, *29*, 11385−11395.
(30) Li, J.; Cassell, A.; Dai, H. Carbon nanotubes as AFM tips: measuring DNA molecules at the liquid/solid interface. *Surf. Interface Anal.* **1999**, *28*, 8−11.
(31) Rabinovich, Y. I.; Daosukho, S.; Byer, K. J.; El-Shall, H. E.; Khan, S. R. Direct AFM measurements of adhesion forces between calcium oxalate monohydrate and kidney epithelial cells in the presence of Ca2+ and Mg2+ ions. *J. Colloid Interface Sci.* **2008**, *325*, 594−601.
(32) Schaefer, J.; Schulze, C.; Marxer, E. E. J.; Schaefer, U. F.; Wohlleben, W.; Bakowsky, U.; Lehr, C.-M. Atomic Force Microscopy and Analytical Ultracentrifugation for Probing Nanomaterial Protein Interactions. *ACS Nano* **2012**, *6*, 4603−4614.
(33) Demokritou, P.; Büchel, R.; Molina, R. M.; Deloid, G. M.; Brain, J. D.; Pratsinis, S. E. Development and characterization of a Versatile Engineered Nanomaterial Generation System (VENGES) suitable for toxicological studies. *Inhal. Toxicol.* **2010**, *22* (Suppl 2), 107−116.
(34) Sotiriou, G. A.; Diaz, E.; Long, M. S.; Godleski, J.; Brain, J.; Pratsinis, S. E.; Demokritou, P. A novel platform for pulmonary and cardiovascular toxicological characterization of inhaled engineered nanomaterials. *Nanotoxicology* **2011**, *6*, 680−690.
(35) Demokritou, P.; Gass, S.; Pyrgiotakis, G.; Cohen, J. M.; Goldsmith, W.; McKinney, W.; Frazer, D.; Ma, J.; Schwegler-Berry, D.; Brain, J.; et al. An in vivo and in vitro toxicological characterisation of realistic nanoscale CeO2 inhalation exposures. *Nanotoxicology* **2013**, *7*, 1338−1350.
(36) Pratsinis, S. E. Flame Aerosol Synthesis of Ceramic Powders. *Prog. Energy Combust. Sci.* **1998**, *24*, 197−219.
(37) Strobel, R.; Pratsinis, S. E. Flame aerosol synthesis of smart nanostructured materials. *J. Mater. Chem.* **2007**, *17*, 4743−4756.
(38) Trovarelli, A. Catalytic properties of ceria and CeO2-containing materials. *Catal. Rev. Sci. Eng.* **1996**, *38*, 439−520.
(39) Gorte, R. J. Ceria in catalysis: From automotive applications to the water−gas shift reaction. *AIChE J.* **2010**, *56*, 1126−1135.
(40) Mai, H.-X.; Sun, L.-D.; Zhang, Y.-W.; Si, R.; Feng, W.; Zhang, H.-P.; Liu, H.-C.; Yan, C.-H. Shape-selective synthesis and oxygen storage behavior of ceria nanopolyhedra, nanorods, and nanocubes. *J. Phys. Chem. B* **2005**, *109*, 24380−24385.
(41) Yabe, S.; Sato, T. Cerium oxide for sunscreen cosmetics. *J. Solid State Chem.* **2003**, *171*, 7−11.
(42) Abiade, J. T.; Yeruva, S.; Choi, W.; Moudgil, B. M.; Kumar, D.; Singh, R. K. A Tribochemical Study of Ceria-Silica Interactions for CMP. *J. Electrochem. Soc.* **2006**, *153*, G1001.
(43) Zhang, H.; He, X.; Zhang, Z.; Zhang, P.; Li, Y.; Ma, Y.; Kuang, Y.; Zhao, Y.; Chai, Z. Nano-CeO2 exhibits adverse effects at environmental relevant concentrations. *Environ. Sci. Technol.* **2011**, *45*, 3725−3730.
(44) Tanner, A. O. Iron Oxide Pigments. In *Minerals Yearbook*; U.S. Geological Survey: Northborough, MA, 2011; Vol. *1*, pp 1−7.
(45) Hilty, F. M.; Arnold, M.; Hilbe, M.; Teleki, A.; Knijnenburg, J. T. N.; Ehrensperger, F.; Hurrell, R. F.; Pratsinis, S. E.; Langhans, W.; Zimmermann, M. B. Iron From Nanocompounds Containing Iron and Zincis Highly Bioavailable in Rats Without Tissue Accumulation. *Nature* **2010**, *5*, 374−380.
(46) Cappella, B.; Dietler, G. Force-distance curves by atomic force microscopy. *Surf. Sci. Rep.* **1999**, *34*, 1−104.
(47) Cross, S. E.; Jin, Y.-S.; Tondre, J.; Wong, R.; Rao, J.; Gimzewski, J. K. AFM-based analysis of human metastatic cancer cells. *Nanotechnology* **2008**, *19*, 384003.
(48) Gad, M.; Itoh, A.; Ikai, A. Mapping cell wall polysaccharides of living microbial cells using atomic force microscopy. *Cell Biol. Int.* **1997**, *21*, 697−706.
(49) Mädler, L.; Stark, W. J.; Pratsinis, S. E. Flame-made ceria nanoparticles. *J. Mater. Res.* **2002**, *17*, 1356−1362.

(50) Wegner, K.; Pratsinis, S. E. Scale-up of nanoparticle synthesis in diusion ame reactors. *Chem. Eng. Sci.* **2003**, *58*, 4581−4589.
(51) Taurozzi, J. S.; Hackley, V. A.; Wiesner, M. R. Ultrasonic dispersion of nanoparticles for environmental, health and safety assessment–issues and recommendations. *Nanotoxicology* **2011**, *5*, 711−729.
(52) DeLoid, G.; Cohen, J. M.; Darrah, T.; Pyrgiotakis, G.; Wohlleben, W.; Demokritou, P. Nanomaterial effective density for *in vitro* dosimetry by volumetric centrifugation. *Nat. Commun.* **2014**, in press.
(53) Giard, D. J.; Aaronson, S. A.; Todaro, G. J.; Arnstein, P.; Kersey, J. H.; Dosik, H.; Parks, W. P. In vitro cultivation of human tumors: establishment of cell lines derived from a series of solid tumors. *J. Nat. Cancer Inst.* **1973**, *51*, 1417.
(54) Ong, Q. K.; Sokolov, I. Attachment of nanoparticles to the AFM tips for direct measurements of interaction between a single nanoparticle and surfaces. *J. Colloid Interface Sci.* **2007**, *310*, 385−390.
(55) Pyrgiotakis, G.; Kundakcioglu, O. E.; Finton, K.; Pardalos, P. M.; Powers, K.; Moudgil, B. M. Cell Death Discrimination with Raman Spectroscopy and Support Vector Machines. *Ann. Biomed. Eng.* **2009**, *37*, 1464−1473.
(56) Pyrgiotakis, G.; Kundakcioglu, O. E.; Pardalos, P. M.; Moudgil, B. M. Raman Spectroscopy and Support Vector Machines for Quick Toxicological Evaluation of Titania Nanoparticles. *J. Raman Spectrosc.* **2011**, *42*, 1222−1231.
(57) Torii, A.; Sasaki, M.; Hane, K.; Okuma, S. A method for determining the spring constant of cantilevers for atomic force microscopy. *Europhys. Lett.* **1999**, *7*, 179−184.
(58) Li, D.; Teoh, W. Y.; Selomulya, C.; Woodward, R. C.; Munroe, P.; Amal, R. Insight into microstructural and magnetic properties of flame-made gamma-Fe2O3 nanoparticles. *J. Mater. Chem.* **2007**, *17*, 4876−4884.
(59) Teleki, A.; Suter, M.; Kidambi, P. R.; Ergeneman, O.; Krumeich, F.; Nelson, B. J.; Pratsinis, S. E. Hermetically coated superparamagnetic Fe2O3 particles with SiO2 nanofilms. *Chem. Mater.* **2009**, *21*, 2094−2100.
(60) Watson, D.; Ge, J.; Cohen, J.; Pyrgiotakis, G.; Engelward, B. P.; Demokritou, P. High Throughput Screening Platform for Engineered Nanoparticle-Mediated Genotoxicity Using CometChip Technology. *ACS Nano* **2014**, *8*, 2118−2133.
(61) Tedja, R.; Lim, M.; Amal, R.; Marquis, C. Effects of Serum Adsorption on Cellular Uptake Profile and Consequent Impact of Titanium Dioxide Nanoparticles on Human Lung Cell Lines. *ACS Nano* **2012**, *6*, 4083−4093.
(62) Johnstone, S. Surface-associated serum proteins inhibit the uptake of phosphatidylserine and poly(ethylene glycol) liposomes by mouse macrophages. *Biochim. Biophys. Acta−Biomembranes* **2001**, *1513*, 25−37.
(63) Lundqvist, M.; Stigler, J.; Elia, G.; Lynch, I.; Cedervall, T.; Dawson, K. Nanoparticle size and surface properties determine the protein corona with possible implications for biological impacts. *Proc. Natl. Acad. Sci. U.S.A.* **2008**, *105*, 14265−14270.
(64) Cedervall, T.; Lynch, I.; Lindman, S.; Berggård, T.; Thulin, E.; Nilsson, H.; Dawson, K. A.; Linse, S. Understanding the nanoparticle-protein corona using methods to quantify exchange rates and affinities of proteins for nanoparticles. *Proc. Natl. Acad. Sci. U.S.A.* **2007**, *104*, 2050−2055.
(65) Lundqvist, M.; Stigler, J.; Cedervall, T.; Berggård, T.; Flanagan, M. B.; Lynch, I.; Elia, G.; Dawson, K. The Evolution of the Protein Corona around Nanoparticles: A Test Study. *ACS Nano* **2011**, *5*, 7503−7509.
(66) Barrán-Berdón, A. L.; Pozzi, D.; Caracciolo, G.; Capriotti, A. L.; Caruso, G.; Cavaliere, C.; Riccioli, A.; Palchetti, S.; Laganà, A. Time Evolution of Nanoparticle-Protein Corona in Human Plasma: Relevance for Targeted Drug Delivery. *Langmuir* **2013**, *29*, 6485−6494.
(67) Dell'Orco, D.; Lundqvist, M.; Oslakovic, C.; Cedervall, T.; Linse, S.; Astier, Y. Modeling the Time Evolution of the Nanoparticle-Protein Corona in a Body Fluid. *PLoS One* **2010**, *5*, 10949.
(68) Satulovsky, J.; Carignano, M. A.; Szleifer, I. Kinetic and thermodynamic control of protein adsorption. *Proc. Natl. Acad. Sci. U.S.A.* **2000**, *97*, 9037−9041.
(69) Vasir, J. K.; Labhasetwar, V. Quantification of the force of nanoparticle−cell membrane interactions and its influence on intracellular trafficking of nanoparticles. *Biomaterials* **2008**, *29*, 4244−4252.
(70) Gass, S.; Cohen, J. M.; Pyrgiotakis, G.; Sotiriou, G. A.; Pratsinis, S. E.; Demokritou, P. A Safer Formulation Concept for Flame-Generated Engineered Nanomaterials. *ACS Sustainable Chem. Eng.* **2013**, *1*, 843−857.